ACS OMEGA

Open Access

http://pubs.acs.org/journal/acsodf

Article

Moringa oleifera Gum-Assisted Synthesis and Characterization of $CoAg_xFe_{2-x}O_4$: Insight into Structural, Magnetic, Optical, and Biomedical Properties

Published as part of ACS Omega virtual special issue "Magnetic Nanohybrids for Environmental Applications".

Qudsiya Y. Tamboli, Sunil M. Patange, Yugal Kishore Mohanta, Asha D. Patil, Rizwan Ali, Ibraheem Bushnak,* and Kranti Zakde*

Cite This: *ACS Omega* 2024, 9, 3835−3845

Read Online

ACCESS | Metrics & More | Article Recommendations

ABSTRACT: The sol−gel method was employed to prepare nano $CoFe_2O_4$ and silver-substituted $CoFe_2O_4$ nanohybrids ($CoAg_xFe_{2-x}O_4$, x = 0, 0.1, 0.2, 0.3, 0.4) utilizing *Moringa oleifera* gum as biofuel. The morphology, size, shape, magnetic, optical, and functional groups of the crystallites were determined using various techniques such as UV−visible, Fourier transform infrared, X-ray diffraction, Rietveld, scanning electron microscopy, transmission electron microscopy, vibrating sample magnetometry, and photoluminescence. The produced nanoferrite has a spherical shape with cubic spinal structures. The optical properties were investigated in two different bands in the photoluminescence emission spectra at 469 and 493 nm. Saturation magnetization (Ms) and coercivity (Hc) decrease as the Ag content increases significantly. Furthermore, antibacterial (Gram-positive bacteria bacterial strains, *Bacillus subtilis* and *Staphylococcus aureus*, and Gram-negative bacterial strains, *Pseudomonas aeruginosa*, and *Escherichia coli*), antibiofilm activity (*E. coli*), and antioxidant (DPPH) activities were investigated. The substantial increase in the silver content offers a constructive impact on studied biomedical activities. These findings encourage additional research into the use of hybrid nanoparticles (an amalgamation of ferrite and a noble metal) in biomedical and pharmaceutical applications.

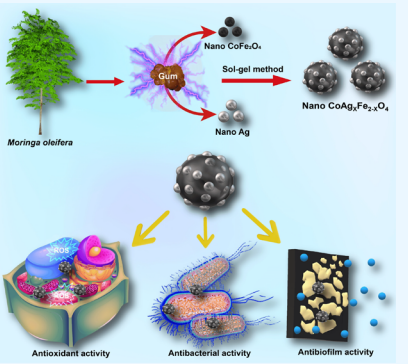

1. INTRODUCTION

Ferrite is a fascinating magnetic material due to its unique properties and applications in biomedical, organic synthesis, optical, magnetic, and electronics. The nanosize ferrites have unlocked multiple possibilities for intensive investigation to establish their antibacterial activities in the field of biomedical applications. Considering the unique properties of cobalt ferrite ($CoFe_2O_4$) nanoparticles[1,2] like ease of synthesis, large magneto crystalline anisotropy, high saturation magnetization (MS), coercivity (HC), high Curie temperature, narrow band gap, excellent permeability, high chemical/electrochemical stability, and mechanical hardness. It is the second most studied magnetic material, with a versatile application in biomedical and industrial fields.[3,4] The preference of metal cations in either the tetrahedral (Td) or octahedral (Oh) sites with composition will determine the magnetic properties of cobalt ferrite. Doping with noble metal cations is the most significant option for boosting the application of $CoFe_2O_4$ in the biomedical field.[5,6]

Silver, gold, palladium, platinum, ruthenium, rhodium, iridium, and rhenium are examples of noble metals. Noble metals, which exhibit exceptional corrosion resistance and high temperature stability, have been successfully used as therapeutic agents in medicine since ancient times. Nanometric noble metals exhibit several uses, especially in biomedicine, where they have the potential to revolutionize many diseases are detected and treated.[6] Multifunctional nanomaterials are entities that combine the remarkable qualities of two or more nanomaterials. Specifically, by adding noble metals and iron oxides to afford diversified nanostructures with enhanced properties.[7]

The rise of antimicrobial-resistant pathogenic bacteria is a significant obstacle in the field of human health. The advent of microorganisms that are resistant to antibiotics has led to a significant increase in severe illnesses, affecting over two million individuals in the United States alone, with an estimated 23,000 fatalities annually.[8] According to recent

Received: October 10, 2023
Revised: December 6, 2023
Accepted: December 18, 2023
Published: January 8, 2024

projections, it has been estimated that by the year 2050, bacterial infections will lead to approximately 10 million deaths annually, surpassing the current number of deaths caused by cancer.[9] Additionally, multiple strains have demonstrated resistance to the latest antibiotics. This information has been documented in previous studies.[10]

Nanomaterials offer a promising avenue for antimicrobial therapies by leveraging structural benefits such as intrinsic composition, morphology, dimensions, and surface properties. Hence, their unique physiochemical characteristics render them a viable option for achieving improved therapeutic outcomes against drug-resistant MDR infections. The proposed mechanism for antimicrobial activity of nanoparticles involved six key postulates: toxic ion release; rupture of the bacterial membrane due to reactive oxygen species (ROS); direct interaction of nanoparticles with bacterial cells (degradation of peptidoglycan layer and cell wall); ROS destroying proteins, RNA, and DNA; bacterial efflux pumps and nanoparticle interaction; and reduction in the synthesis of adenosine triphosphate (ATP) inside the cell.[11] A potentially important factor in the defense mechanism of bacterial biofilms is the production of glycolipid and glycoprotein coatings that encircle the cell layers of bacteria and make it easier for bacterial cell growth inside the biofilm to avoid resistance from the host and the action of antibacterial factors.[12] Nanotechnology may offer an opportunity by penetrating biofilms and inhibiting biofilm development.

Literature data revealed that silver nanoparticles (Ag NPs) exhibit excellent antimicrobial activity compared to other metal nanoparticles.[13] In addition to the characteristic antimicrobial properties of silver, recent studies revealed that the antibacterial activity of $CoFe_2O_4$ will be enhanced by the addition of Ag.[14] Hence, the investigation of novel antibacterial nanomaterials and the exploration of the new properties of hybrid materials have become attractive research areas. Therefore, to recognize the most effective nanoscale ferrite materials, researchers study various combinations of cobalt ferrite and silver metal to evaluate their antibacterial properties against various bacterial strains.

The antibacterial properties of the ferrite nanoparticles are significantly dependent on their size and morphology. Therefore, a synthetic methodology plays a crucial role in tuning these parameters. However, most conventional methods are expensive and hazardous to the environment. The extensive use of the sol−gel method has been well documented in the literature as quick, easy, and economical.[15] Moreover, natural organisms and natural substances such as plant extracts have been effectively utilized for the green synthesis of nanocobalt ferrite as a cheap and eco-friendly process.[16] There is significantly less research in the literature on green synthesis of silver−cobalt ferrite nanoparticles like Okra (*A. esculentus*) plant extract,[17] honey,[18] flower and leaf extracts of *Hibiscus rosa-sinensis*,[19] extracts from tulsi seed (*Ocimum sanctum*),[20] *Citrus limon*,[21,22] and egg-white[23−25] compared with conventional synthesis techniques. Additionally, several studies have reported the green synthesis of metal nanoparticles using a variety of plant gums and resins.[15,26] *Moringa oleifera* is a medicinal plant from the *Moringaceae* family. It is popularly known as the drumstick tree or the miracle tree in India. The various sections of *Moringa* were successfully used for the green synthesis of metal and metal oxide nanomaterials.[21] Recently, *M. oleifera* leaf extract[27−30] and gum[26] were successfully utilized for the synthesis of silver nanoparticles (AgNPs). However, *M. oleifera* gum-assisted sol-gel synthesis of the Ag-substituted nano $CoFe_2O_4$ and the subsequent synergistic effect of increasing percentages of Ag on various bacterial strains have not been reported yet.

Herein, we aim to provide phytochemically assisted green synthesis, structural characterization, and antibacterial/antibiofilm/antioxidant effects of the various silver concentrations (x = 0, 0.1, 0.2, 0.3, and 0.4) on cobalt ferrite. *M. oleifera* gum was successfully utilized as a green fuel in sol−gel synthesis, and resulting biosynthesized hybrid nano ferrites were characterized by XRD, UV, SEM, FTIR, and TEM. The magnetic and photoluminescence properties were evaluated through VSM and UV, respectively. The antibacterial and antibiofilm activities against Gram-positive and Gram-negative bacteria was studied. Moreover, the antioxidative properties were also evaluated through the radical scavenging method, as shown in Figure 1.

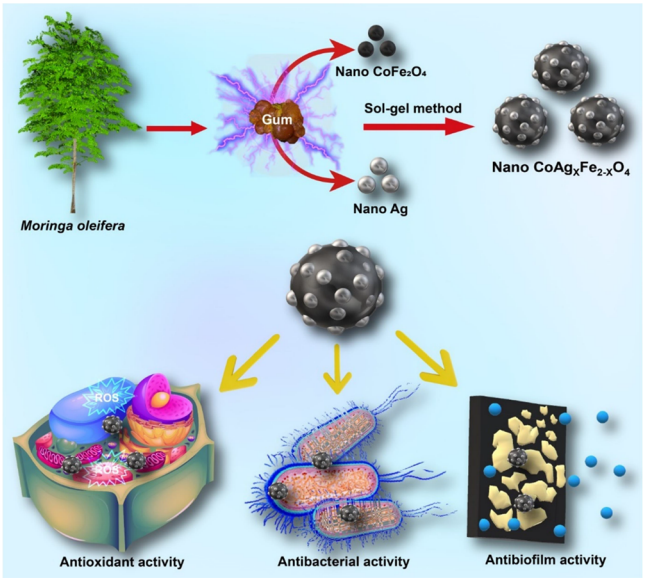

Figure 1. Greener synthesis and applications of $CoAg_xFe_{2-x}O_4$ nano hybrid.

2. RESULTS AND DISCUSSION

2.1. X-ray Diffraction Analysis. The X-ray diffraction technique was used to confirm the formation of phase in synthesized cobalt ferrite and Ag-substituted cobalt ferrite nanohybrids; the investigated diffraction patterns are shown in Figure 2. In the diffraction pattern, the identified peaks are indexed as (220), (311), (222), (400), (422), (511), and (440), corresponding to cubic spinel structures with space group Fd3m.

The FullProf Suite software was utilized for the Rietveld refinement XRD data, and the obtained parameters such as goodness of fit (χ^2), expected R values (R_{ex}), and weighted profile R-factor (R_{wp}) are summarized in Table 1. The investigation of Rietveld refinement shows the formation of a secondary phase having an Fm3m space group along with the spinel phase for the cobalt ferrite samples substituted with Ag. Lattice constant values along with the relative percentage of the two phases (spinel and Ag) formed within the ferrites are given in Table 1. Furthermore, from Table 2, it is found that there is a simultaneous decline in the spinel phase from 89 to

https://doi.org/10.1021/acsomega.3c06578
ACS Omega 2024, 9, 3835−3845

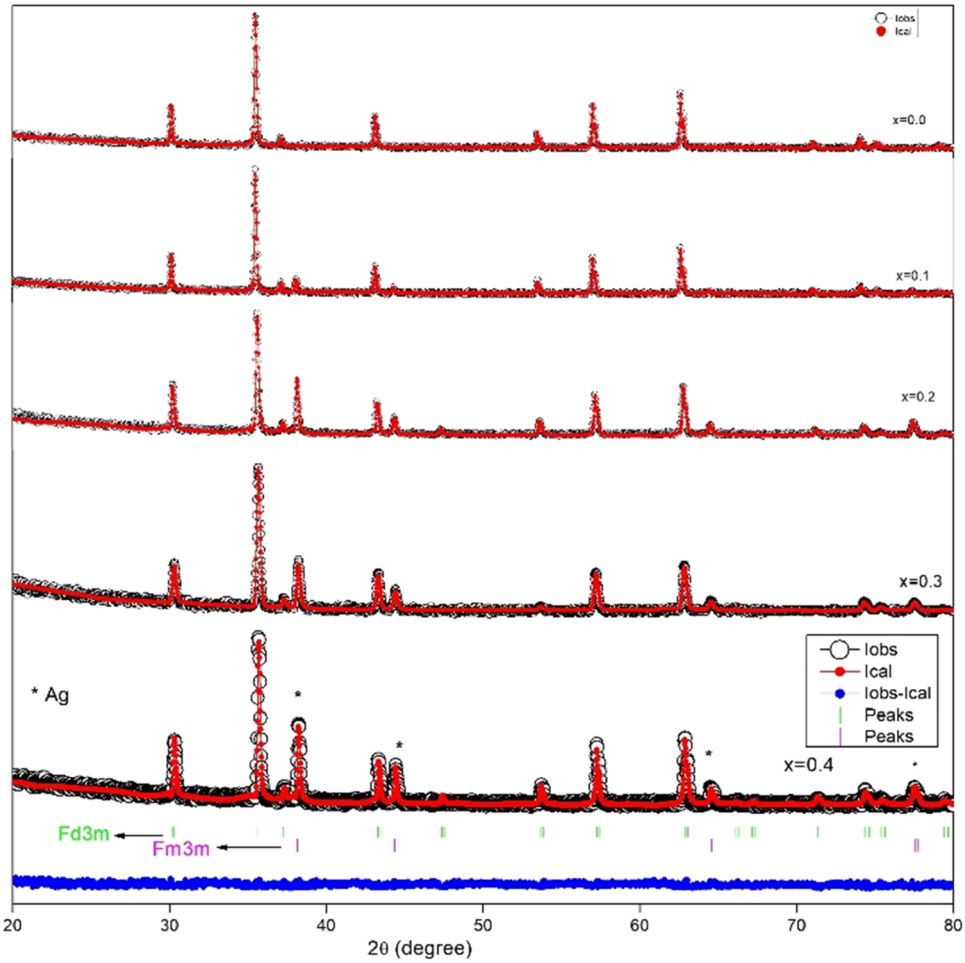

Figure 2. Rietveld refined XRD spectra of $CoAg_xFe_{2-x}O_4$. The vertical lines in green and pink at the bottom of the XRD indicate the positions of Bragg's peaks.

Table 1. Discrepancy Factor (R_{wp}), Expected Values (R_{exp}), and Goodness of Fit (χ^2) for $Co_1Ag_xFe_{2-x}O_4$

nanoferrites	R_{wp}	R_{exp}	χ^2
QT1 ($CoFe_2O_4$)	10.3	10.5	1.02
QT2 ($Co_1Ag_{0.1}Fe_{1.9}O_4$)	14.1	14.5	1.05
QT3 ($Co_1Ag_{0.2}Fe_{1.8}O_4$)	13.6	14.6	1.14
QT4 ($Co_1Ag_{0.3}Fe_{1.7}O_4$)	15.4	19.1	1.53
QT5 ($Co_1Ag_{0.4}Fe_{1.6}O_4$)	14.8	16.5	1.23

Table 2. Lattice Constant, Spinel Phase %, and Ag Phase % for $Co_1Ag_xFe_{2-x}O_4$

	lattice constant			
nanoferrites	spinel phase	Ag phase	spinel phase % (Fd3m)	Ag phase % (Fm3m)
QT1 ($CoFe_2O_4$)	8.3873		100	
QT2 ($Co_1Ag_{0.1}Fe_{1.9}O_4$)	8.3855	4.0897	89	11
QT3 ($Co_1Ag_{0.2}Fe_{1.8}O_4$)	8.3729	4.0857	80	20
QT4 ($Co_1Ag_{0.3}Fe_{1.7}O_4$)	8.3618	4.0843	75	25
QT5 ($Co_1Ag_{0.4}Fe_{1.6}O_4$)	8.3614	4.0819	72	28

72%, with enhancement in the secondary phase from 11 to 28% which indicates that Ag molecules may surround the Fe^{3+} cations at the sublattice sites.

The lattice parameter values of the investigated samples were obtained from the eq 1:

$$a = d\sqrt{h^2 + k^2 + l^2} \quad (1)$$

where h, k, l = Miller indices, d = interplanar spacing.

It is observed (Table 2) that the decrease in lattice parameter values corresponds to an increment of the silver content in cobalt ferrite, which is due to the greater ionic radius of the silver ion than the cobalt ion. Furthermore, due to their inability to diffuse within the spinel lattice, silver ions with large ionic radii form secondary phases on the grain boundaries.[31]

Using the Debye–Scherrer formula, the crystallite sizes (D) of samples were determined by eq 2:

$$D = \frac{0.9\lambda}{\beta\cos\theta} \quad (2)$$

where λ = X-rays wavelength (1.540562 Å), β = full width at half-maximum (fwhm) and θ = Bragg's diffraction angle.

2.2. FESEM Analysis. Figure 3 represents field-emission scanning electron microscopy (FESEM) images of $CoAg_xFe_{2-x}O_4$ (x = 0, 0.1, 0.2, 0.3 concentration). From these images, it can be observed that the synthesized nanohybrids exhibit a spherical shape and agglomerate because of magnetic interactions. The investigated agglomerated structures showed a nonuniform distribution of hybrids in the prepared samples.

https://doi.org/10.1021/acsomega.3c06578
ACS Omega 2024, 9, 3835−3845

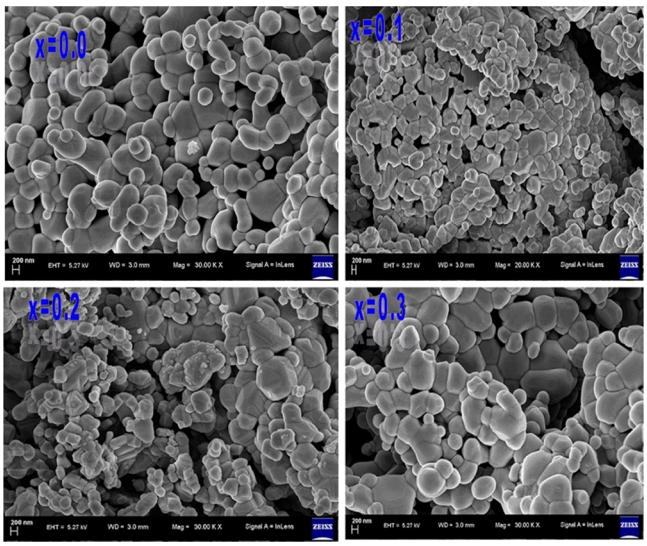

Figure 3. FESEM images of $CoAg_xFe_{2-x}O_4$ ferrites.

2.3. TEM Analysis. The shape and size properties of synthesized nanoferrite can be better understood by combining the TEM image with the particle size distribution histogram. Transmission electron microscopy (TEM) images obtained after ultrasonic treatment in ethanol for 15 min (Figure 4) show the morphologies and particle sizes of $Co_1Ag_{0.2}Fe_{1.8}O_4$. The image shows that the morphology of some of the nanoparticles resembles an irregular shape, with most of the nanocrystals in a monosized and spherical shape. The nanoparticles modestly aggregated. By size counting from the appropriate TEM image, the size distributions of the nanocrystals were determined. These patterns of size distribution were well-fitted by Gaussian distributions, providing an average diameter of 30 nm. A fair distribution of particle-like characteristics could be seen that provides further understanding of the crystallinity of the nano ferrite. The high crystalline characteristics of the Ag-substituted ferrite were confirmed by the distinguished and uniform lattice fringes.

2.4. FTIR Analysis. Figure 5 reveals Fourier transform infrared (FTIR) spectra for cobalt ferrite samples substituted

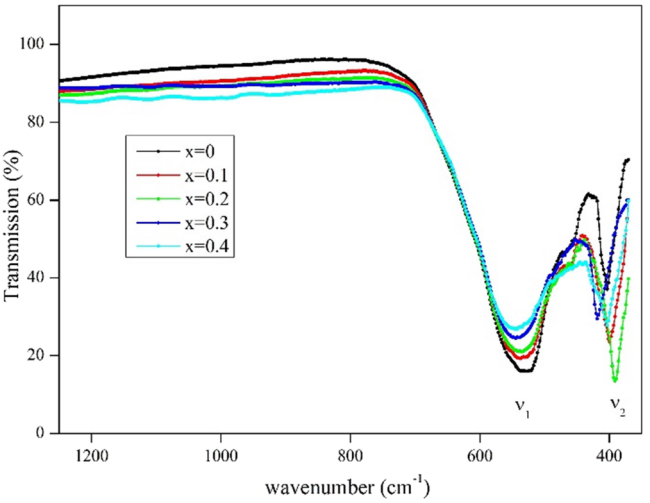

Figure 5. FTIR spectra of $Co_1Ag_xFe_{2-x}O_4$ ferrites.

with various compositions of Ag in the range 1200−400 cm^{-1}. It provides crucial information for understanding the composition and behavior of cobalt ferrite hybrids by molecular vibrations, the spinel ferrite structure confirmation, and insights into the structural modifications induced by the substitution of Ag. In FTIR spectra, two peaks below 1000 cm^{-1} are found, which are distinctive features of the spinel ferrites.[32] The peaks observed in the range of 391−418 cm^{-1} in each sample are attributed to vibrations of octahedral metal−oxygen bonds, signifying the interaction between cobalt ions and oxygen atoms in the octahedral coordination environment. The peak at 534−553 cm^{-1} corresponds to vibrations of tetrahedral metal−oxygen bonds, revealing the arrangement of cobalt ions and oxygen atoms in the tetrahedral coordination

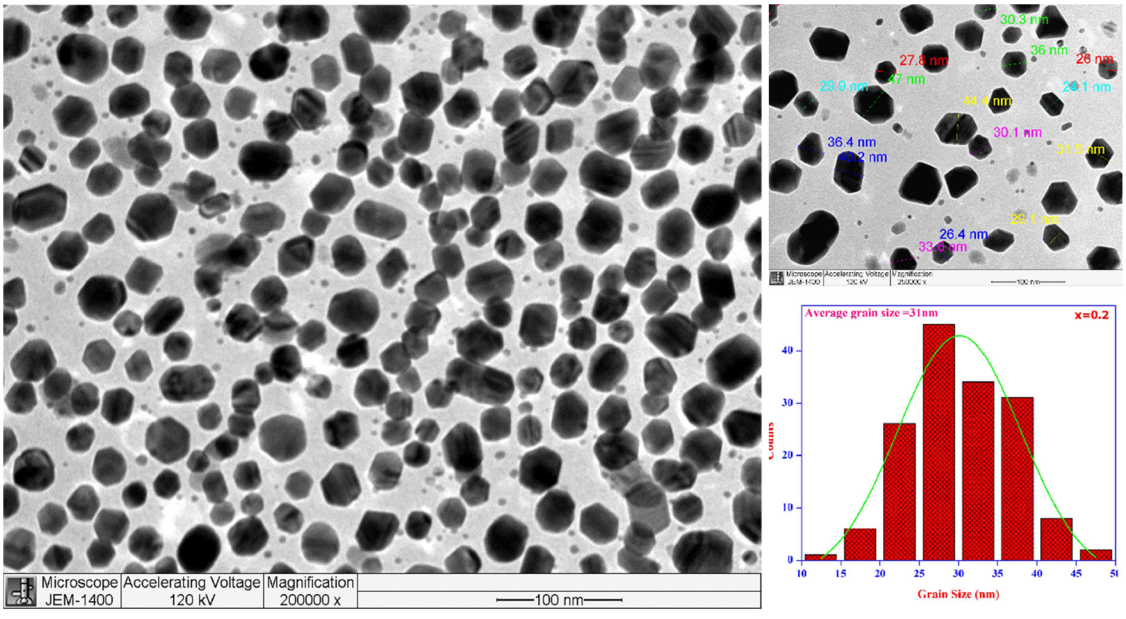

Figure 4. TEM image and particle size distribution histogram of $Co_1Ag_{0.2}Fe_{1.8}O_4$.

https://doi.org/10.1021/acsomega.3c06578
ACS Omega 2024, 9, 3835−3845

sites. The existence of these peaks confirms the formation of the spinel ferrite structure in newly prepared ferrite hybrids. Table 3 provides a detailed analysis of peak positions with

Table 3. Values of Absorption Bands (ν_1 and ν_2) and Band Gap Energy for $Co_1Ag_xFe_{2-x}O_4$

nanoferrites	vibrational frequency (cm^{-1}) ν_1	ν_2	band gap energy E_g (eV)
QT1 ($CoFe_2O_4$)	534	391	2.12
QT2 ($Co_1Ag_{0.1}Fe_{1.9}O_4$)	538	399	2.34
QT3 ($Co_1Ag_{0.2}Fe_{1.8}O_4$)	540	403	2.52
QT4 ($Co_1Ag_{0.3}Fe_{1.7}O_4$)	548	405	2.70
QT5 ($Co_1Ag_{0.4}Fe_{1.6}O_4$)	553	418	2.90

silver (Ag) substitution in cobalt ferrite. The observed slight variation in peak positions suggests changes in the local environment of metal−oxygen bonds. This variation can be attributed to the redistribution or migration of cations between the tetrahedral and octahedral sites within the crystal lattice. This process indicates the interaction and integration of Ag into cobalt ferrite.

2.5. Optical Properties. The optical properties of Ag-substituted cobalt ferrite nanohybrids prepared by the sol−gel method were studied by UV−visible spectroscopy to understand the energy levels associated with the electronic transitions. The position and nature of the absorption edges provide information about the energy required for electronic transitions. The absorption peaks correspond to the promotion of electrons from lower to higher energy orbitals. UV−vis spectroscopy can reveal size-dependent effects as well as photocatalytic activity.

The absorption spectra of all samples were performed in the range 200−800 nm and are shown in Figure 6. The studied ferrites exhibit visible-region absorption in their acquired spectra.

The band gap energy (E_g) values were obtained by using the Tauc eq 3

$$\alpha h\nu^n = A(h\nu - E_g)^n \quad (3)$$

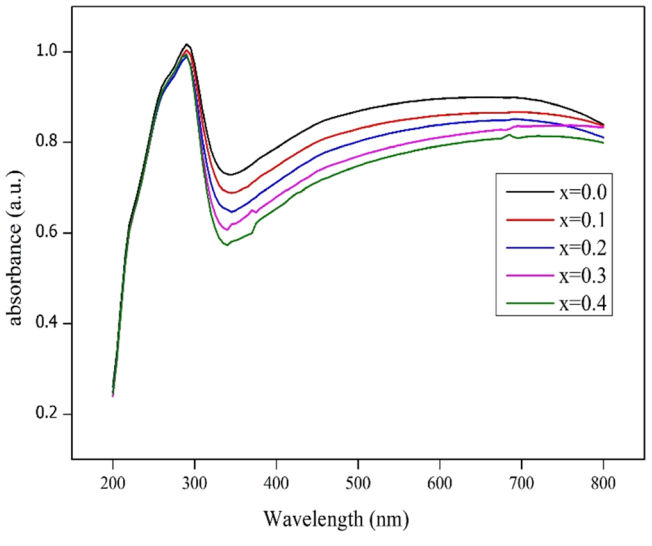

Figure 6. UV−vis absorbance spectra of $Co_1Ag_xFe_{2-x}O_4$ ferrites.

where E_g = optical band gap energy and h = Planck's constant

The energy band gap is a critical optical property. Depending on the crystal structure and composition, cobalt ferrite may have both direct and indirect band gaps. The band gap energy influences the ability of cobalt ferrite to absorb and emit light, an essential property for electronic and optoelectronic applications. The band gap energies of prepared cobalt ferrite samples with different contents of Ag doping were obtained by plotting graphs between the direct band gap $(\alpha h\nu)^2$ and photon energy $(h\nu)$, as shown in Figure 7. The

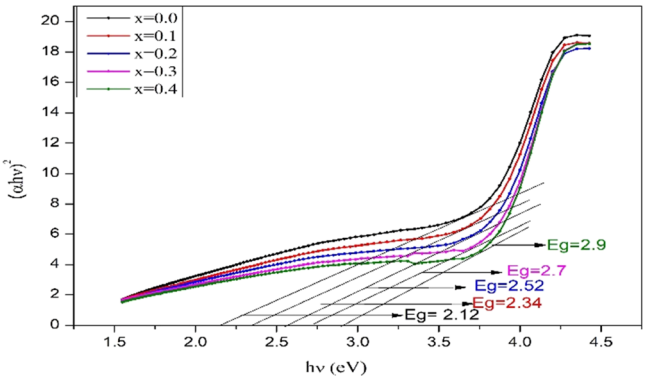

Figure 7. Tauc plots of $Co_1Ag_xFe_{2-x}O_4$ nanoferrites.

band gap energy can be obtained by extra plotting the linear part to $(\alpha h\nu)^2 = 0$. The computed values of the band gap energies are depicted in Table 3. From Table 3, it is found that band gap energy values are enhanced with the content of Ag in cobalt ferrite samples, which is related to the particle size of the prepared ferrite samples.[33]

2.6. Magnetic Properties. The response of the magnetization of $Co_1Ag_xFe_{2-x}O_4$ NPs with an applied magnetic field at room temperature is studied with the help of a vibrating sample magnetometer. The hysteresis loops for different contents of Ag in cobalt ferrite are represented in Figure 8, which gives the relation between magnetization and the applied magnetic field. The hysteresis loops appear to be wide, which indicates that all of the samples show a hard magnetic

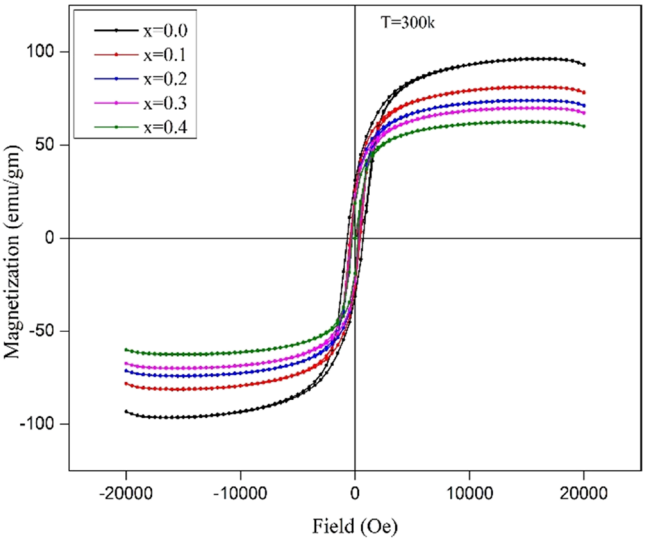

Figure 8. Room-temperature magnetic hysteresis loops for $Co_1Ag_xFe_{2-x}O_4$.

https://doi.org/10.1021/acsomega.3c06578
ACS Omega 2024, 9, 3835−3845

character. The values of coercivity (Hc) and saturation magnetization (Ms) were obtained from the hysteresis loops and are shown in Figure 9. It is noticed that saturation

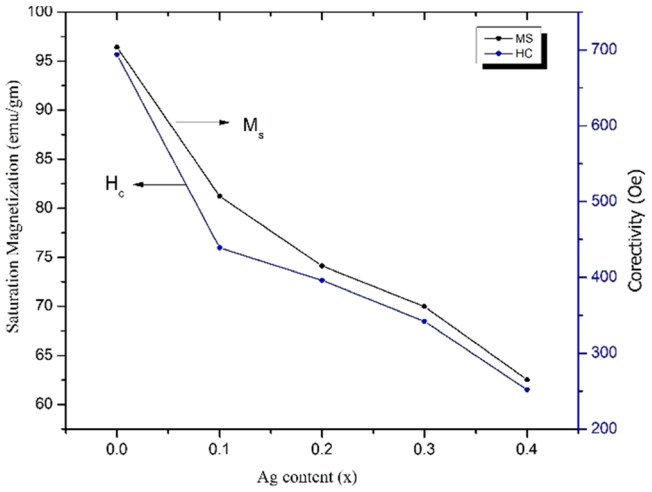

Figure 9. Variation of saturation magnetization and coercivity of $Co_1Ag_xFe_{2-x}O_4$.

magnetization decreases with enhancement in the concentration of Ag in cobalt ferrite, which is owing to the replacement of the Co^{2+} ion with the nonmagnetic Ag^+ ion.[34]

In the present study, iron has a 5 μB magnetic moment, which is equally distributed at octahedral as well as tetrahedral sites, and cobalt ions with a 3 μB magnetic moment occupy the octahedral site, whereas silver ions with a 0 μB magnetic moment prefer to occupy the B-site and replace some of the cobalt ions at the A-site, resulting in a decrease in saturation magnetization, which results in the reduction of the magnetic moment at the octahedral B site, as shown in Figure 9. Furthermore, this can be explained with the help of Neel's theory[35] and the super-exchange interaction mechanism. It is observed that as the amount of Ag in cobalt ferrites increases, the coercivity (Hc) values decrease, which corresponds to a decrease in crystallite size and anisotropy.[36] Particle size, morphology, microstrain, magneto-crystalline anisotropy, ionic radii, and the type of metal ions are some of the factors that affect coercivity (Hc).[37,38]

2.7. Photoluminescence (PL) Analysis. PL properties of the $CoAg_xFe_{2-x}O_4$ nanohybrid have been studied at room temperature and shown in Figure 10 as excitation and emission photoluminescence spectra. The electron−hole recombination rate of the samples was studied at room temperature with the help of photoluminescence spectra. It is well-known that an elevated surface-to-volume ratio in nanocrystalline ferrite promotes oxygen vacancies and defects by bond cleavage. A newly synthesized hybrid material behaves in a similar manner. Monovalent Ag^+ ions replace Fe^{2+} ions to create an imbalance in charge. This change can subsequently lead to more defects in the $CoFe_2O_4$ lattice. It is obvious that the spectrum exhibits a broad emission peak at 469 nm, which may result from the recombination of holes and electrons in the conduction and valence bands. This is appropriate for deep traps of lattice defects with limited surface conditions.[39] The origin of luminous characteristics in the nanomaterial lattice is due to such forces.

2.8. Antibacterial Activity. The bactericidal activity of silver-substituted cobalt ferrite nanohybrids synthesized using

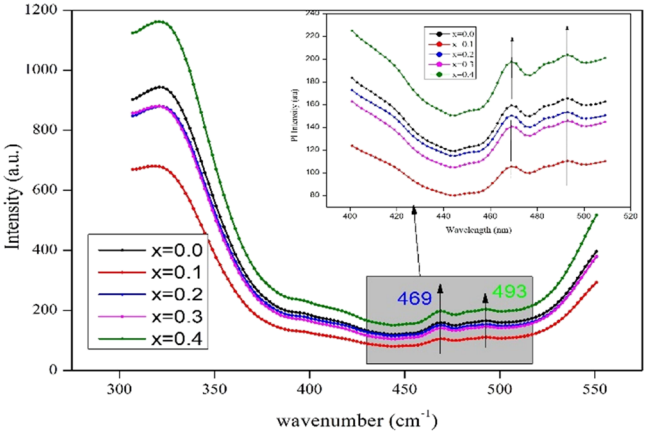

Figure 10. PL spectra of $Co_1Ag_xFe_{2-x}O_4$ ferrites.

M. oleifera gum was determined against Gram-positive and Gram-negative bacteria, revealing a dose-dependent relationship. For the preliminary screening regarding their antibacterial activity, the zone of inhibition was measured and is depicted in Table 4. The antibacterial activity is higher in QT5 ($Co_1Ag_{0.4}Fe_{1.6}O_4$) against *B. subtilis* and *E. coli* as compared to the lower percentage of Ag-substituted, but in the case of *S. aureus* and *P. aeruginosa*, QT5 has less activity as compared to its lower concentrations. Sometimes, in the agar well diffusion method, there is variability in the diffusion potential of the samples. However, in the broth dilution method, where the MIC was calculated, the results revealed an increase in the antibacterial potential as a function of the percentage of Ag-substituted cobalt ferrite (Table 5). The detail of the dose-dependent antibacterial activities of silver-substituted cobalt ferrite nanohybrids is depicted in the Supporting Information. It may be due to appropriate interaction between the nanohybrids and bacterial cells under the solution conditions.

For effective antibacterial activity, the appropriate interaction between the cells and compounds or samples should be required, and it might have been possible with the broth dilution method, which showed interesting antibacterial results in the current experiment. Hence, *M. oleifera* gum-assisted synthesis of silver-substituted nano cobalt ferrite exhibits potential antimicrobial activities. The current finding supports the hypothesis in accordance with literature reports. Hence, the current synthesized silver-substituted cobalt ferrite nanohybrids would be a better option as a material to be utilized for different applications in the era of multidrug resistance.

2.9. Antibiofilm Activity. *M. oleifera* gum-assisted synthesized silver-substituted nanocobalt ferrites have also been assayed for antibiofilm activity against biofilm-forming bacteria. In the present study, the in vitro antibiofilm activity of $Co_1Ag_xFe_{2-x}O_4$ was evaluated in a dose-dependent manner against the biofilm-forming bacteria *E. coli*. The individual species of bacteria were grown in 96-well microtiter plates for 24 h, and then treatments of 1000 μg/mL of the individual synthesized $Co_1Ag_xFe_{2-x}O_4$ ferrites were added to each well. Results of the assay revealed that the biosynthesized $Co_1Ag_xFe_{2-x}O_4$ ferrites inhibited biofilm formation by the bacterial species, relative to the negative control used in the experiment (Figure 11). The MICs of antibiofilm activity of QT5 ($Co_1Ag_{0.4}Fe_{1.6}O_4$) and Streptomycin were expressed in terms of IC_{50} and found to be 774.08 ± 42.86 and 578.71 ± 9.22 μg/mL respectively (Table 6). From the MIC value, it

https://doi.org/10.1021/acsomega.3c06578
ACS Omega 2024, 9, 3835−3845

Table 4. Antibacterial Activity of $Co_1Ag_xFe_{2-x}O_4$ in Agar Well Diffusion Methods with Results Represented as Zone of Inhibition (in mm ± S.D.)

strain name	QT1	QT2	QT3	QT4	QT5	standard (sterptomycin)
S. aureus	17.00 ± 0.08	22.00 ± 0.00	16.00 ± 0.00	21.00 ± 0.00	15.00 ± 0.00	18.00 ± 0.00
P. aeruginosa	20.90 ± 0.12	20.00 ± 0.08	26.00 ± 0.08	19.00 ± 0.08	17.00 ± 0.08	24.00 ± 0.00
B. subtilis	17.03 ± 0.04	21.00 ± 0.00	16.00 ± 0.00	19.00 ± 0.00	22.00 ± 0.00	24.00 ± 0.00
E. coli	17.09 ± 0.04	19.03 ± 0.04	20.63 ± 0.51	18.00 ± 0.08	22.00 ± 0.08	22.00 ± 0.00

Table 5. Anti-bacterial Activity of $Co_1Ag_xFe_{2-x}O_4$ with MIC Results Represented as μg/mL ± S.D.

nanoferrites	IC_{50}(μg/mL)			
	S. aureus	*P. aeruginosa*	*B. subtilis*	*E. coli*
QT1 ($CoFe_2O_4$)	194.05 ± 11.22	139.03 ± 5.12	156.11 ± 9.83	134.5 ± 2.18
QT2 ($Co_1Ag_{0.1}Fe_{1.9}O_4$)	64.78 ± 1.01	67.81 ± 2.70	66.60 ± 2.28	69.33 ± 1.92
QT3 ($Co_1Ag_{0.2}Fe_{1.8}O_4$)	42.54 ± 0.79	66.73 ± 1.84	32.36 ± 0.60	66.84 ± 1.00
QT4 ($Co_1Ag_{0.3}Fe_{1.7}O_4$)	32.95 ± 0.75	61.48 ± 2.76	21.48 ± 0.15	21.36 ± 0.48
QT5 ($Co_1Ag_{0.4}Fe_{1.6}O_4$)	25.45 ± 1.06	28.12 ± 0.96	16.16 ± 0.37	20.50 ± 2.74

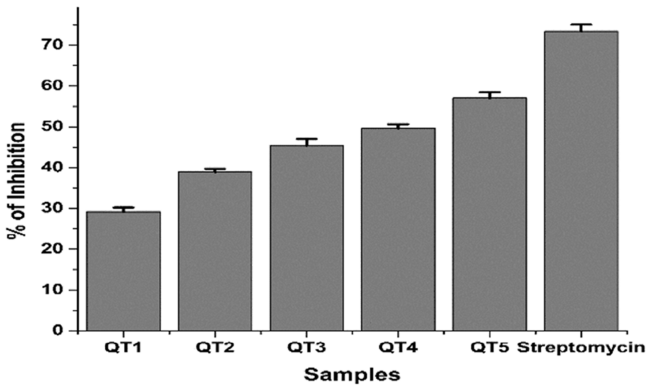

Figure 11. Antibiofilm activity of $Co_1Ag_xFe_{2-x}O_4$ nano ferrites.

was clearly indicated that silver-substituted cobalt ferrite nanohybrids can be used as a strong antibiofilm agent against biofilm-forming pathogenic bacteria. Moreover, the addition of *M. oleifera* gum as the reducing and capping agent will be another valuable addition to safer nano ferrite development. The current study supports the literature data that suggests metal-substituted cobalt ferrite nanoparticles have potential antibiofilm activity. Hence, the current finding recommends the potential possibilities of using $Co_1Ag_xFe_{2-x}O_4$ ferrites in antibiofilm eradication.[40]

2.10. Antioxidant Activity. There have been several research reports on the individual antioxidant properties of silver and cobalt ferrite nanoparticles. The antioxidant capability, which was assessed using the DPPH assay as a model reaction, showed that cobalt ferrite nanoparticles exhibit good antioxidant potential compared to ascorbic acid.[41,42] Likewise, individual silver nanoparticles and also silver have several reports on potential DPPH scavenging activities.[13] Therefore, the significant antioxidant potential of $Co_1Ag_xFe_{2-x}O_4$ ferrites was evaluated by the DPPH radical scavenging assay, and significant scavenging potentials were found in all combinations of nano ferrites with increasing order (Figure 12). QT5 ($Co_1Ag_{0.4}Fe_{1.6}O_4$) was found to inhibit 69.34 ± 1.53% which is nearest to the value of the positive control, Ascorbic acid (73.76 ± 1.17%).

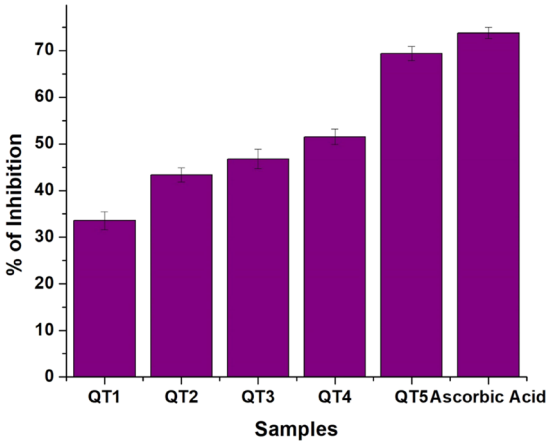

Figure 12. Antioxidant activity of $Co_1Ag_xFe_{2-x}O_4$ nanoferrites.

The results give a good indication that $Co_1Ag_xFe_{2-x}O_4$ in cellular systems has a lower risk. From the results, it was clearly indicated that silver-substituted cobalt ferrites can be used as biologically susceptible and safe materials in future applications related to living cells. In the present study, the same results as in the literature report the potentiality of antioxidant activity through DPPH radical scavenging activities. The current results strongly establish the potential of $Co_1Ag_xFe_{2-x}O_4$ ferrites for different biomedical applications.

3. CONCLUSIONS

We successfully demonstrated the utilization of aqueous *M. oleifera* gum extract as a biofuel for the synthesis of cubic spinal Ag-substituted cobalt ferrite ($Co_1Ag_xFe_{2-x}O_4$) with nonuniformly distributed spherically shaped nanohybrids. The XRD

Table 6. MIC (IC_{50} μg/mL) of $Co_1Ag_xFe_{2-x}O_4$ against Biofilm-Forming Bacteria *E. coli*

samples	1000 μg/mL	500 μg/mL	250 μg/mL	125 μg/mL	IC_{50}μg/mL
QT5 ($Co_1Ag_{0.4}Fe_{1.6}O_4$)	57.05 ± 1.63	35.50 ± 1.79	19.25 ± 0.97	9.54 ± 0.92	774.08 ± 42.86
streptomycin	73.76 ± 1.63	53.11 ± 1.36	31.79 ± 1.22	14.21 ± 1.60	578.71 ± 9.22

https://doi.org/10.1021/acsomega.3c06578
ACS Omega 2024, 9, 3835−3845

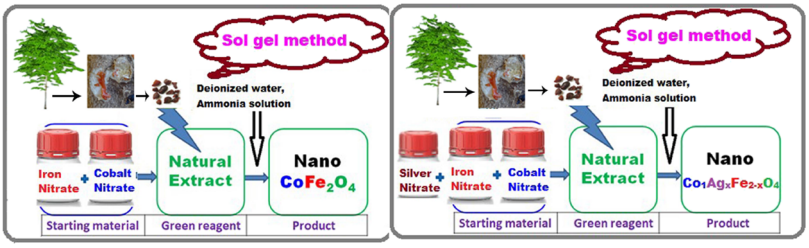

Figure 13. *M. oleifera* gum-assisted synthesis of $CoAg_xFe_{2-x}O_4$.

pattern confirmed the formation of the spinel structure, with the second phase having space group fm3m. It is specified that the lattice constant increases with an increase in the concentration of Ag. The substantial increase in the silver content offers a constructive impact on optical properties. The VSM investigation indicates that coercivity (Hc) and saturation magnetization (Ms) decline with an increase in the silver percentage. The enhanced antimicrobial, antibiofilm, and antioxidative properties were predominantly attained by augmenting surface reactivity via appropriate surface area and nanoscale dimensions. It became apparent that the quantity of silver in cobalt ferrite subsequently enhanced the antibacterial properties. The current study's findings can be expanded to examine the inhibition of multidrug-resistant bacteria by combining varied amounts of silver with different ferrite nanoparticles.

4. MATERIALS AND METHODS

4.1. Chemicals and Reagents. The analytical-grade reagents were purchased from Sigma-Aldrich: ferric nitrate nonahydrate ($Fe(NO_3)_3{\cdot}9H_2O$), cobalt nitrate hexahydrate ($Co(NO_3)_2{\cdot}6H_2O$), silver nitrate ($AgNO_3$), and ammonia solution (NH_4OH).

4.2. Preparation of *Moringa oleifera* Gum Extract. Using a mortar and pestle, 10 g of *M. oleifera* gum was crushed to a fine powder. The powder was dissolved in 100 mL of deionized water and heated for 2 h while being continuously stirred. The aqueous solution was filtered using Whatman No. 1 filter paper, cooled to room temperature, and stored for future use.

4.3. Preparation of Ag-Substituted Cobalt Ferrite Nanohybrids. Silver-substituted cobalt ferrite nanohybrids with the composition of $CoAg_xFe_{2-x}O_4$ (x = 0, 0.1, 0.2, 0.3, 0.4) were synthesized by the sol−gel method, as shown in Figure 13. The compound was prepared by mixing a stoichiometric ratio of ferric nitrate, cobalt nitrate, and silver nitrate and dissolving it in deionized water. Aqueous *M. oleifera* gum extract was used as a biofuel and added to the prepared aqueous solution in a molar ratio of 1:1. The pH of the solution was adjusted by dropwise addition of ammonia solution to 7 under stirring. The obtained solution was placed on a hot plate at 80 °C to afford a thick viscous gel, which was subsequently removed by extended heating to furnish a ferrite powder. The obtained powder was crushed to a fine powder with an agate mortar. Finally, the fine powder was subjected to calcination at 600 °C for 5 h in a temperature-controlled furnace.

4.4. Characterization. The XRD spectra of calcined samples were obtained using a Bruker D2 PHASER X-ray diffractometer with Cu Kα as the radiation source, which has a wavelength of λ = 1.5405 Å and is inclined at diffraction angles of 2θ between 20° and 80° at room temperature. The samples' microstructures were examined using FESEM (FEI Nova Nano SEM 450). TEM images were acquired using a Gatan camera and TEM Center Ver.1.4.3222 (TEM operating and acquisition system) on a JEOL-JEM 1400 operating at 120 kV. Using a Jasco FT/IR 4000 series spectrometer, a Fourier transform infrared (FTIR) spectroscopic analysis was performed. Magnetic analysis was studied using a vibrating sample magnetometer (Quantum Design PPMS-VSM) at room temperature. Using a UV/vis spectrophotometer, we investigated the optical characteristics of the samples were investigated.

4.5. Antibacterial Activity. The antibacterial activities of $CoAg_xFe_{2-x}O_4$ nano ferrites were carried out following the methods described by in the literature.[13] Briefly, the antibacterial activity of the synthesized nanohybrids was conducted by using simple and familiar agar-well diffusion methods. During the activity test, the Muller-Hinton Agar (MHA) medium was used for the growth of the test pathogenic bacteria. Broth (100 μL) of each bacterial strain such as *S. aureus* (ATCC 25923), *P. aeruginosa* (ATCC 15442), *B. subtilis* (ATCC 6051), and *E. coli* (ATCC 25922), was spread over the medium uniformly. Wells with a diameter of 5 mm were created through the utilization of a sterile cork borer. Preparations were made by dissolving all nanocomposites (1000 μg/mL) in DMSO, followed by the addition of 10 μL of each individual nanocomposite into the designated well. Additionally, the Petri plates that were subjected to inoculation were placed in an incubator set at a temperature of 37 °C for a duration of 24 h. The streptomycin solution, with a concentration of 1000 μg/mL, was prepared as a positive control, while dimethyl sulfoxide (DMSO) was selected as the negative control. The assessment of antibacterial activity involved the quantification of the zone of inhibition (ZI) diameters. All of the determinations were conducted in triplicate, ensuring the replication of each experiment for increased statistical robustness. Furthermore, the minimum inhibitory concentration (MIC) of $CoAg_xFe_{2-x}O_4$ nanohybrids was evaluated.[43] The minimum inhibitory concentrations (MICs) of $CoAg_xFe_{2-x}O_4$ nano ferrites were quantified and represented as an IC_{50} value. All experimental procedures were conducted in triplicate, and subsequently, the mean value and standard deviation were computed.

4.6. Antibiofilm Activity. A 96-well microtiter plate (flat bottom, polystyrene) was used to determine the antibiofilm activity of the Ag-substituted cobalt ferrite nanohybrids.[43,44] In a sterile 96-well microtiter, plates containing 100 μL of Nutrient broth per well and 50 μL of fresh bacterial suspension (*E. co* Gram-negative) were added. 100 μL of standard (Streptomycin 1000 μg/mL) solution was added to the standard test. In each test well, 100 μL of the samples containing Ag-substituted cobalt ferrite nanoparticles at a concentration of 1000 μg/mL were introduced. Following a

https://doi.org/10.1021/acsomega.3c06578
ACS Omega 2024, 9, 3835−3845

period of incubation at a temperature of 37 °C for 24 h, the contents of each well were delicately extracted by tapping the plates. The wells underwent a thorough washing process using 200 μL of sterile saline solution in order to eliminate any bacteria that were not attached to a surface. The formation of biofilms by cells that adhere to the plate was facilitated, followed by staining using a 0.1% concentration of crystal violet. The resulting biofilms were then incubated at ambient temperature for 20 min. The surplus stain was eliminated through a thorough rinsing process employing deionized water, while the plates were subsequently treated with 200 μL of 96% ethanol for fixation. The optical densities (OD) of stained bacteria that adhere to surfaces were quantified at a wavelength of 630 nm using an enzyme-linked immunosorbent assay (ELISA) microplate reader. The percentage of inhibition of biofilm formation was calculated using the following eq 4:

$$\%\ \text{biofilm inhibition} = [1 - (\text{OD}_{630}\ \text{of cells treated with Nano hybrids}/\text{OD}_{630}\ \text{of the non} - \text{treated control}) \times 100] \quad (4)$$

The experiments were performed in triplicate, and the average value along with the standard deviation was calculated.

4.7. Antioxidant Activity. Antioxidant activity in the sample QT1, QT2, QT3, QT4, and QT5 compounds was estimated for their free radical scavenging activity by using DPPH (1, 1-Diphenyl-2, Picryl-Hydrazyl) free radicals.[44] A total volume of 100 μL of QT1, QT2, QT3, QT4, and QT5 nanohybrids, each with a concentration of 1000 μ/ml, were aliquoted into the microtiter plate. A volume of 100 μL of a methanolic solution containing 0.1% of DPPH (2,2-diphenyl-1-picrylhydrazyl) was introduced onto the samples, followed by an incubation period of 30 min under light-restricted conditions. Ascorbic acid was utilized as the positive control. The samples were subsequently subjected to a visual examination for any alterations in coloration. The transition from a purple hue to yellow and pale pink shades was deemed indicative of robust and feeble positive reactions, respectively. The Elisa plate reader was employed to analyze the plate at a wavelength of 490 nm, enabling the determination of radical scavenging activity by the following eq 5:

$$\text{DPPH radical scavenging activity}\ (\%) = [(\text{Absorbance of control} - \text{Absorbance of test sample})/(\text{Absorbance of control})] \times 100 \quad (5)$$

4.8. Statistical Analysis. The determination of the statistical significance in the data was achieved through analysis utilizing the Duncan test. The data are displayed in the format of mean ± standard deviation (SD). The observed data exhibited statistical significance with a p value of less than 0.05.

AUTHOR INFORMATION

Corresponding Authors

Ibraheem Bushnak − *King Abdullah International Medical Research Center (KAIMRC), King Saud Bin Abdulaziz University for Health Sciences, Ministry of National Guard-Health Affairs, Riyadh 14811, Saudi Arabia*; Email: BushnakIb@mngha.med.sa

Kranti Zakde − *Department of Basic and Applied Science, MGM University, Aurangabad 431001 Maharashtra, India*; orcid.org/0000-0002-4446-5227; Email: kzakde@mgmu.ac.in

Authors

Qudsiya Y. Tamboli − *Department of Basic and Applied Science, MGM University, Aurangabad 431001 Maharashtra, India*

Sunil M. Patange − *Materials Science Research Laboratory, SKM, Osmanabad 413613 Maharashtra, India*

Yugal Kishore Mohanta − *Nano-Biotechnology and Translational Knowledge Laboratory, Department of Applied Biology, School of Biological Sciences, University of Science and Technology Meghalaya, Techno City 793101 Meghalaya, India; Centre for Herbal Pharmacology and Environmental Sustainability, Chettinad Hospital and Research Institute, Chettinad Academy of Research and Education, Chennai 603103 Tamil Nadu, India*; orcid.org/0000-0002-6547-7227

Asha D. Patil − *Deshbhakt Anandrao Balawantrao Naik Art's and Science College, Sangli 415408 Maharashtra, India*

Rizwan Ali − *King Abdullah International Medical Research Center (KAIMRC), King Saud Bin Abdulaziz University for Health Sciences, Ministry of National Guard-Health Affairs, Riyadh 14811, Saudi Arabia*

Complete contact information is available at: https://pubs.acs.org/10.1021/acsomega.3c06578

Author Contributions

The manuscript was written through the contributions of all authors. All authors have given approval to the final version of the manuscript

Notes

The authors declare no competing financial interest.

ACKNOWLEDGMENTS

The authors would like to acknowledge the Department of Physics, MGM University, Aurangabad, India, for consumables and experimental facilities. The authors would like to thank Dr. Yasinalli Tamboli for his help in manuscript writing.

REFERENCES

(1) Jauhar, S.; Kaur, J.; Goyal, A.; Singhal, S. Tuning the Properties of Cobalt Ferrite: A Road towards Diverse Applications. *RSC Adv.* **2016**, *6* (100), 97694−97719.

(2) Amiri, S.; Shokrollahi, H. The Role of Cobalt Ferrite Magnetic Nanoparticles in Medical Science. *Mater. Sci. Eng. C* **2013**, *33* (1), 1−8.

(3) Tatarchuk, T. R.; Paliychuk, N. D.; Bououdina, M.; Al-Najar, B.; Pacia, M.; Macyk, W.; Shyichuk, A. Effect of Cobalt Substitution on Structural, Elastic, Magnetic and Optical Properties of Zinc Ferrite Nanoparticles. *J. Alloys Compd.* **2018**, *731*, 1256−1266.

(4) Alves, T. E. P.; Pessoni, H. V. S.; Franco, A. The Effect of Y3+ Substitution on the Structural, Optical Band-Gap, and Magnetic Properties of Cobalt Ferrite Nanoparticles. *Phys. Chem. Chem. Phys.* **2017**, *19* (25), 16395−16405.

(5) Satheeshkumar, M. K.; Kumar, E. R.; Indhumathi, P.; Srinivas, C.; Deepty, M.; Sathiyaraj, S.; Suriyanarayanan, N.; Sastry, D. L. Structural, morphological and magnetic properties of algae/CoFe2O4 and algae/Ag-Fe-O nanocomposites and their biomedical applications. *Inorg. Chem. Commun.* **2020**, *111*, No. 107578.

(6) Rai, M.; Ingle, A. P.; Birla, S.; Yadav, A.; Santos, C. A. D. Strategic Role of Selected Noble Metal Nanoparticles in Medicine. *Crit. Rev. Microbiol.* **2016**, *42* (5), 696−719.

(7) Liu, X.; Iocozzia, J.; Wang, Y.; Cui, X.; Chen, Y.; Zhao, S.; Li, Z.; Lin, Z. Noble Metal-Metal Oxide Nanohybrids with Tailored

Nanostructures for Efficient Solar Energy Conversion, Photocatalysis and Environmental Remediation. *Energy Environ. Sci.* **2017**, *10* (2), 402−434.
(8) *FY15 Detect and Protect Against Antibiotic Resistance Budget Initiative*; Atlanta, GA, 2003. http://www.cdc.gov/drugresistance/threat-report-2013/pdf/FY15-DPAR-budget-init.pdf.
(9) Willyard, C. The Drug-Resistant Bacteria That Pose the Greatest Health Threats. *Nature* **2017**, *543* (7643), 15.
(10) Ventola, C. L. The Antibiotic Resistance Crisis: Part 1: Causes and Threats. *P T* **2015**, *40* (4), 277−283.
(11) Sanchez, L. M.; Alvarez, V. A. Advances in Magnetic Noble Metal/Iron-Based Oxide Hybrid Nanoparticles as Biomedical Devices. *Bioengineering* **2019**, *6* (3), 75.
(12) Costerton, J. W.; Cheng, K. J.; Geesey, G. G.; Ladd, T. I.; Nickel, J. C.; Dasgupta, M.; Marrie, T. J. Bacterial Biofilms in Nature and Disease. *Annu. Rev. Microbiol.* **1987**, *41*, 435−464.
(13) Mohanta, Y. K.; Nayak, D.; Mishra, A. K.; Chakrabartty, I.; Vasanthakumaran, M.; Muthupandian, S.; Murugan, K.; Sharma, G. Green Synthesis of Endolichenic Fungi Functionalized Silver Nanoparticles: The Role in Antimicrobial, Anti-Cancer, and Mosquitocidal Activities. *IJMS* **2022**, *23* (18), 10626.
(14) Kooti, M.; Saiahi, S.; Motamedi, H. Fabrication of Silver-Coated Cobalt Ferrite Nanocomposite and the Study of Its Antibacterial Activity. *J. Magn. Magn. Mater.* **2013**, *333*, 138−143.
(15) Tamboli, Q. Y.; Patange, S. M.; Mohanta, Y. K.; Sharma, R.; Zakde, K. R. Green Synthesis of Cobalt Ferrite Nanoparticles: An Emerging Material for Environmental and Biomedical Applications. *J. Nanomater.* **2023**, *2023*, No. 9770212.
(16) Gul, I. H.; Maqsood, A. Structural, Magnetic and Electrical Properties of Cobalt Ferrites Prepared by the Sol-Gel Route. *J. Alloys Compd.* **2008**, *465* (1−2), 227−231.
(17) Routray, K. L.; Saha, S.; Behera, D. Insight Into the Anomalous Electrical Behavior, Dielectric and Magnetic Study of Ag-Doped CoFe2O4 Synthesised by Okra Extract-Assisted Green Synthesis. *J. Electron. Mater.* **2020**, *49* (12), 7244−7258.
(18) Satheeshkumar, M. K.; Kumar, E. R.; Srinivas, C.; Suriyanarayanan, N.; Deepty, M.; Prajapat, C. L.; Rao, T. V. C.; Sastry, D. L. Study of Structural, Morphological and Magnetic Properties of Ag Substituted Cobalt Ferrite Nanoparticles Prepared by Honey Assisted Combustion Method and Evaluation of Their Antibacterial Activity. *J. Magn. Magn. Mater.* **2019**, *469*, 691−697.
(19) Gingasu, D.; Mindru, I.; Patron, L.; Calderon-Moreno, J. M.; Mocioiu, O. C.; Preda, S.; Stanica, N.; Nita, S.; Dobre, N.; Popa, M.; Gradisteanu, G.; Chifiriuc, M. C. Green Synthesis Methods of $CoFe_2O_4$ and Ag-$CoFe_2O_4$ Nanoparticles Using Hibiscus Extracts and Their Antimicrobial Potential. *J. Nanomater.* **2016**, *2016*, No. 106756.
(20) Mahajan, P.; Sharma, A.; Kaur, B.; Goyal, N.; Gautam, S. Green Synthesized (Ocimum Sanctum and Allium Sativum) Ag-Doped Cobalt Ferrite Nanoparticles for Antibacterial Application. *Vacuum* **2019**, *161*, 389−397.
(21) Abdelsattar, A. S.; Kamel, A. G.; El-Shibiny, A. The green production of eco-friendly silver with cobalt ferrite nanocomposite using Citrus limon extract. *Results Chem.* **2023**, *5*, No. 100687.
(22) Priya, R. S.; Chaudhary, P.; Kumar, E. R.; Balamurugan, A.; Srinivas, C.; Prasad, G.; Yadav, B. C.; Sastry, D. L. Evaluation of structural, dielectric and electrical humidity sensor behaviour of $MgFe_2O_4$ ferrite nanoparticles. *Ceram. Int.* **2021**, *47* (11), 15995−16008.
(23) Kumar, E. R.; Kamzin, A. S.; Janani, K. Effect of annealing on particle size, microstructure and gas sensing properties of Mn substituted CoFe2O4 nanoparticles. *J. Magn. Magn. Mater.* **2016**, *417*, 122−129.
(24) Kumar, E. R.; Jayaprakash, R.; Patel, R. Structural and morphological studies of manganese substituted $CoFe_2O_4$ and $NiFe_2O_4$ nanoparticles. *Superlattices Microstruct.* **2013**, *62*, 277−284.
(25) Kumar, E. R.; Jayaprakash, R.; Kumar, S. The role of annealing temperature and bio template (egg white) on the structural, morphological and magnetic properties of manganese substituted MFe2O4 (M= Zn, Cu, Ni, Co) nanoparticles. *J. Magn. Magn. Mater.* **2014**, *351*, 70−75.
(26) Irfan, M.; Munir, H.; Ismail, H. Moringa Oleifera Gum Based Silver and Zinc Oxide Nanoparticles: Green Synthesis, Characterization and Their Antibacterial Potential against MRSA. *Biomater. Res.* **2021**, *25* (1), 17.
(27) Kannan, M.; Govindaraju, K.; Elango, K.; Kalyanasundaram, M.; Lakshmanan, A. Biogenic Nanomaterials Using Moringa and Their Applications. In *The Moringa Genome. Compendium of Plant Genomes*; Springer: Cham, 2021; pp 157−165. DOI: 10.1007/978-3-030-80956-0_13.
(28) Puspitarum, D. L.; Istiqomah, N. I.; Tumbelaka, R. M.; Kusumaatmaja, A.; Oshima, D.; Kato, T.; Suharyadi, E. High Performance of Magnetically Separable and Recyclable Photocatalyst of Green-Synthesized CoFe2O4/TiO2 Nanocomposites for Degradation of Methylene Blue. *Adv. Nat. Sci. Nanosci. Nanotechnol.* **2022**, *13* (4), No. 045003.
(29) Moodley, J. S.; Krishna, S. B. N.; Pillay, K.; Govender, P.; Sershen. Green Synthesis of Silver Nanoparticles from Moringa Oleifera Leaf Extracts and Its Antimicrobial Potential. *Adv. Nat. Sci. Nanosci. Nanotechnol.* **2018**, *9* (1), No. 015011.
(30) Amina, M.; Al Musayeib, N. M.; Alarfaj, N. A.; El-Tohamy, M. F.; Orabi, H. E.; Bukhari, S. I.; Mahmoud, A. Z. Exploiting the Potential of Moringa Oleifera Oil/Polyvinyl Chloride Polymeric Bionanocomposite Film Enriched with Silver Nanoparticles for Antimicrobial Activity. *Int. J. Polym. Sci.* **2019**, *2019*, No. 678149.
(31) Kumar, E. R.; Srinivas, C.; Seehra, M. S.; Deepty, M.; Pradeep, I.; Kamzin, A. S.; Mehar, M. V. K.; Mohan, N. K. Particle Size Dependence of the Magnetic, Dielectric and Gas Sensing Properties of Co Substituted NiFe2O4 Nanoparticles. *Sensors Actuators, A Phys.* **2018**, *279*, 10−16.
(32) Sanpo, N.; Berndt, C. C.; Wang, J. Microstructural and Antibacterial Properties of Zinc-Substituted Cobalt Ferrite Nanopowders Synthesized by Sol-Gel Methods. *J. Appl. Phys.* **2012**, *112* (8), No. 084333.
(33) Jayakumar, T.; Rajeevgandhi, C.; Anand, P. Effect on Magnetic Behaviour of Ag and Cd Doped Cobalt Ferrite Nanoparticles Prepared by Glycine-Assisted Sol-Gel Auto Combustion Method. *J. Alloys Compd.* **2023**, *962*, No. 171098.
(34) Ali, M. D.; Zeeshan, T.; Tahir, W. Impact of Silver Substitution on Structural, Magnetic, Optical and Antibacterial Properties of Cobalt Ferrite. *SSRN Electron. J.* **2022**, No. 167650.
(35) Pawar, R. A.; Patange, S. M.; Tamboli, Q. Y.; Ramanathan, V.; Shirsath, S. E. Spectroscopic, elastic and dielectric properties of Ho3+ substituted Co-Zn ferrites synthesized by sol-gel method. *Ceram. Int.* **2016**, *42* (14), 16096−16102.
(36) Patange, S. M.; Shirsath, S. E.; Jangam, G. S.; Lohar, K. S.; Jadhav, S. S.; Jadhav, K. M. Rietveld Structure Refinement, Cation Distribution and Magnetic Properties of Al3+ Substituted NiFe2O4 Nanoparticles. *J. Appl. Phys.* **2011**, *109* (5), No. 053909.
(37) Cullity, B. D.; Graham, C. D. Introduction to Magnetic Materials. *Introd. to Magn. Mater.* **2008**, No. 386323.
(38) Pawar, R. A.; Desai, S. S.; Tamboli, Q. Y.; Shirsath, S. E.; Patange, S. M. Ce3+ incorporated structural and magnetic properties of M type barium hexaferrites. *J. Magn. Magn. Mater.* **2015**, *378*, 59−63.
(39) Almessiere, M. A.; Slimani, Y.; Baykal, A. Structural and Magnetic Properties of Ce-Doped Strontium Hexaferrite. *Ceram. Int.* **2018**, *44* (8), 9000−9008.
(40) Mohanta, Y. K.; Chakrabartty, I.; Mishra, A. K.; Chopra, H.; Mahanta, S.; Avula, S. K.; Patowary, K.; Ahmed, R.; Mishra, B.; Mohanta, T. K.; Saravanan, M.; Sharma, N. Nanotechnology in Combating Biofilm: A Smart and Promising Therapeutic Strategy. *Front. Microbiol.* **2023**, *13*, No. 028086.
(41) El-Sayed, E.-S. R.; Abdelhakim, H. K.; Zakaria, Z. Extracellular Biosynthesis of Cobalt Ferrite Nanoparticles by Monascus Purpureus and Their Antioxidant, Anticancer and Antimicrobial Activities: Yield Enhancement by Gamma Irradiation. *Mater. Sci. Eng., C* **2020**, *107*, No. 110318.

https://doi.org/10.1021/acsomega.3c06578
ACS Omega 2024, 9, 3835−3845

(42) Panda, J.; Das, S.; Kumar, S.; Tudu, B.; Sarkar, R. Investigation of Antibacterial, Antioxidant, and Anticancer Properties of Hydrothermally Synthesized Cobalt Ferrite Nanoparticles. *Appl. Phys. A Mater. Sci. Process.* **2022**, *128* (7), 1.
(43) Mohanta, Y.; Biswas, K.; Jena, S.; Hashem, A.; Mohanta, T.; Abd Allah, E. Anti-Biofilm and Antibacterial Activities of Silver Nanoparticles Synthesized by the Reducing Activity of Phytoconstituents Present in the Indian Medicinal Plants. *Front. Microbiol.* **2020**, *11*, 1784.
(44) Mohanta, Y.; Panda, S.; Biswas, K.; Tamang, A.; Bandyopadhyay, J.; De, D.; Bastia, A.; Mohanta, D. Biogenic Synthesis of Silver Nanoparticles from Cassia Fistula (Linn.): In Vitro Assessment of Their Antioxidant, Antimicrobial and Cytotoxic Activities. *IET Nanobiotechnol.* **2016**, *10* (6), 438−444, DOI: 10.1049/iet-nbt.2015.0104.

https://doi.org/10.1021/acsomega.3c06578
ACS Omega 2024, 9, 3835−3845